A Study of the Design and Stability of One Dimensional Hydrogen-Bonded Nanotubes

A Thesis submitted to

Indian Institute of Science Education and Research, Pune

In partial fulfilment of the requirements for the BS-MS Dual Degree Programme

By

Abhradeep Sarkar

Reg. No.: 20191003

Indian Institute of Science Education and Research Pune

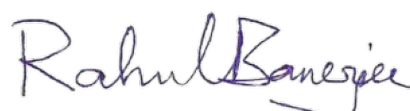Dr. Homi Bhabha Road,

Pashan, Pune 411008, India.

April, 2024

Supervisor: **Prof. Rahul Banerjee**

Indian Institute of Science Education and Research Kolkata

CERTIFICATE

This is to certify that this dissertation entitled **"A Study of the Design and Stability of One Dimensional Hydrogen-Bonded Nanotubes"** towards the partial fulfilment of the BS-MS dual degree programme at the Indian Institute of Science Education and Research, Pune represents study/work carried out by **Abhradeep Sarkar** at Indian Institute of Science Education and Research Kolkata under the supervision of **Prof. Rahul Banerjee,** Professor, Department of Chemical Sciences, IISER Kolkata during the academic year 2023-2024.
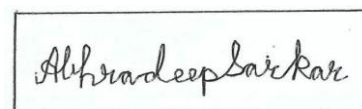
Prof. Rahul Banerjee

May 2024

Committee:

Prof. Rahul Banerjee

Prof. Ramanathan Vaidhyanathan

Dedicated to my parents and sister for their support throughout.

DECLARATION

I hereby declare that the matter embodied in the report entitled **"A Study of the Design and Stability of One Dimensional Hydrogen-Bonded Nanotubes"** are the results of the work carried out by me at the Department of Chemical Sciences, Indian Institute of Science Education and Research (IISER) Kolkata, under the supervision of Prof. Rahul Banerjee, and the same has not been submitted elsewhere for any other degree. Wherever others contribute, every effort is made to indicate this clearly, with due reference to the literature and acknowledgement of collaborative research and discussions.

Abhradeep Sarkar

May 2024

Acknowledgments

I would like to extend my deep sense of gratitude to my respected faculty advisor, **Prof. Rahul Banerjee**, for the opportunity to work in his lab and for his continued support and encouragement throughout the past few months. I would also like to thank my TAC Expert member, **Prof. Ramanathan Vaidhyanathan,** for his valuable feedback on my thesis.

Thereafter, I was fortunate enough to be assigned to work with **Dr. Kalipada Koner**, who helped me within and outside the lab and expedited the development of ideas that resulted in this thesis. It also would never have been possible without input and support from the PMATLab members and new friends I made at IISER-K especially Sabyasachi da, Rohan da, Shibani di, Amit, and Soumyadeep.

I am also glad to have wonderful friends at IISER Pune who were always ready to listen to my problems and have interesting and meaningful discussions – Abhijit, Ranojoy, Shayandeep, Ashutosh, Trupti, Abhinav, Vaishak, and Ashmi.

Next, I would like to thank the **Department of Chemical Sciences (DCS) at Indian Institute of Science Education and Research (IISER) Kolkata** for providing a high-quality research atmosphere and a chance to participate in it, and the **Department of Chemistry at IISER Pune** for helping me pursue my dreams.

I am also grateful to **Kishore Vaigyanik Protsahan Yojana (KVPY)** for funding my studies and supporting my dreams.

Last but not the least, I will always be indebted to my parents and sister for their continued support over the years.

Table of Contents

List of Tables

List of Figures

b) Possible packing of the compound into a hexagonal nanotube – Page 39

List of Abbreviations

ATR – Attenuated Total Reflection – Page 17

BLYP – Becke, Lee, Yang and Parr functional – Page 20

CAN – Ceric ammonium nitrate – Page 17

CNT – Carbon nanotube – Page 12

CONT – Covalent organic nanotube – Page 12

DCM – Dichloromethane – Page 17

DMF – Dimethyl formamide – Page 19

DMSO – Dimethyl sulfoxide – Page 21

DFT – Density Functional Theory – Page 11

HONT – Hydrogen-bonded Organic Nanotube – Page 11

IEFPCM – Integral Equation Formalism Polarizable Continuum Model – Page 20

IR – Infrared spectroscopy – Page 17

LDA – Local density approximation – Page 20

MHz – Megahertz – Page 17

NMR – Nuclear Magnetic Resonance experiment – Page 17

Pd/C – Palladium on activated charcoal – Page 18

SCXRD – Single crystal X-ray diffraction experiment – Page 17

TAT – Triptycene tetraamine – Page 11

TAT-Im – *2,8*-bis(*2*-methoxyphenyl)-*1,5,7,11*-tetrahydro-*5,11-[1,2]b*enzenoanthra[*2,3-d:6,7-d'*] diimidazole – Page 11

TLC – Thin layer chromatography – Page 18

THF – Tetrahydrofuran – Page 21

UV – Ultraviolet light – Page 18

Abstract

Nanotubes are a novel class of materials that show unique properties due to their one-dimensional backbone. Hydrogen-bonded organic nanotubes (HONTs) are among the most promising supramolecular nanotubes because of their structural resemblance with biologically active tubular channels. Most reported HONTs are prepared from large building blocks such as macrocyclic compounds and peptides, which demands complicated synthetic procedures.

In this work, we designed and synthesized a triptycene-based building block, *2,8-*bis(*2-methoxyphenyl)-1,5,7,11-*tetrahydro-*5,11-[1,2]* benzenoanthra[*2,3-d:6,7-d'*] diimidazole, abbreviated as **TAT-Im**, through a bottom-up multi-step process from triptycene with tetraamino triptycene (TAT) as an intermediate. TAT-Im was thereafter used to synthesize a tetragonal hydrogen-bonded nanotube.

Chapter 1 of the thesis provides a brief overview of nanotubes, especially with respect to supramolecular nanotubes. We then discuss the significance of weak hydrogen bonds in literature to provide context for additional stability in supramolecular structures. In **Chapter 2**, we discuss the synthetic route of TAT-Im alongside the design of the computational calculation experiments. **Chapter 3** provides insight on the characterization of intermediates, and the various crystal structures of TAT-Im in different solvent systems. We also explore the possibilities laid out from the DFT calculation analysis. Finally, **Chapter 4** summarizes the discussions carried out in previous chapters and emphasizes the possible directions for studying one-dimensional supramolecular systems.

Chapter 1

Introduction

1.1 Nanotubes

One Dimensional Organic Nanotubes
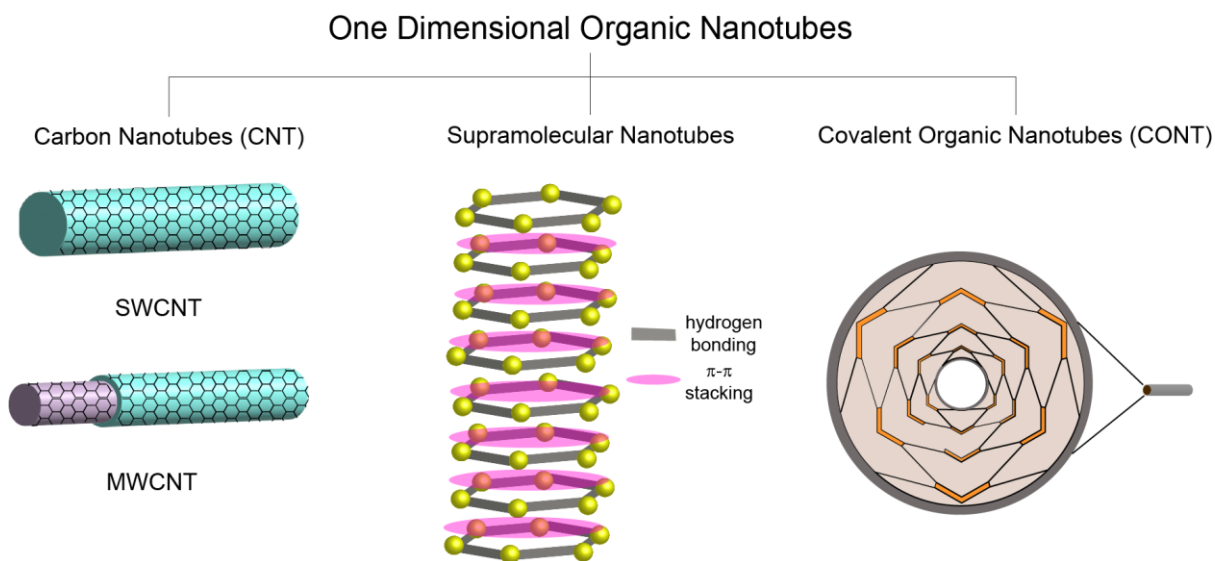
Fig.1.1: Classification of One-Dimensional Organic Nanotubes into Carbon Nanotubes, Supramolecular Nanotubes and Covalent Organic Nanotubes

Nanotubes are one-dimensional nanomaterials with hollow channels that grow in a particular direction, and the diameter of such channels lies in the nanometre region, that is, of the order of 10^{-9} m. The dimensionality and distinctive structure of such materials has led to some unique properties and applications like energy storage, heterogenous catalysis and drug delivery. These applications are highly dependent on diameter, length and more importantly the structural stability which is governed by the nature of connectivity. Depending on connectivity, nanotubes can be divided into inorganic, metal-organic or purely organic. However, considerable efforts have been made over the last decade to design and synthesize organic nanotubes, probably to avoid the toxicity and limited scope of functionalization associated with metal-based nanotubes.

Carbon nanotubes (CNTs) are certainly the most explored organic nanotubes due to their impressive stability and superior conductivity. It was first synthesized by Sumio Ijima in 1991 in the multi-walled carbon nanotube form (MWCNT) *via* the arc discharge method[1]. Till today, the synthesis of carbon nanotubes requires sophisticated techniques like chemical vapor deposition, laser ablation and arc discharge.

Arc discharge involves passing direct current between graphite electrodes in a helium chamber at extremely harsh conditions of temperature above 1500°C and low pressure[2]. Laser ablation also entails accurate control of several variables, such as the laser intensity and wavelength, the buffer gas and the target material[3]. Even the modern method of synthesizing carbon nanotubes, chemical vapor deposition, requires fairly high temperatures of around 600°C[4]. Another drawback of carbon

nanotubes is their low solubility in both organic and aqueous solvents, forming aggregates and making it difficult to perform functional group modifications easily[5]. The functionalization routes explored involve reactions on a defect site[6], which adversely affects the efficacy of these materials[7]. Despite these shortcomings, carbon nanotubes are widely used in gas sensors[8], water purification[9], electronics[10], and the textile industry.

Over time, other organic nanotubes including supramolecular nanotubes and covalent organic nanotubes have garnered interest to address the limitations of CNTs. These nanotubes often have a comparatively simple synthetic route beginning from commonly available ligands and can even be prepared at room temperature. Among them, supramolecular nanotubes are an interesting class due to their structural flexibility that is comparable to various biological systems. The design of such nanotubes, however, requires careful choice of starting materials based on their symmetry and position of functional groups to form selectively designed nanotubes.

1.2 Hydrogen-bonded Nanotubes
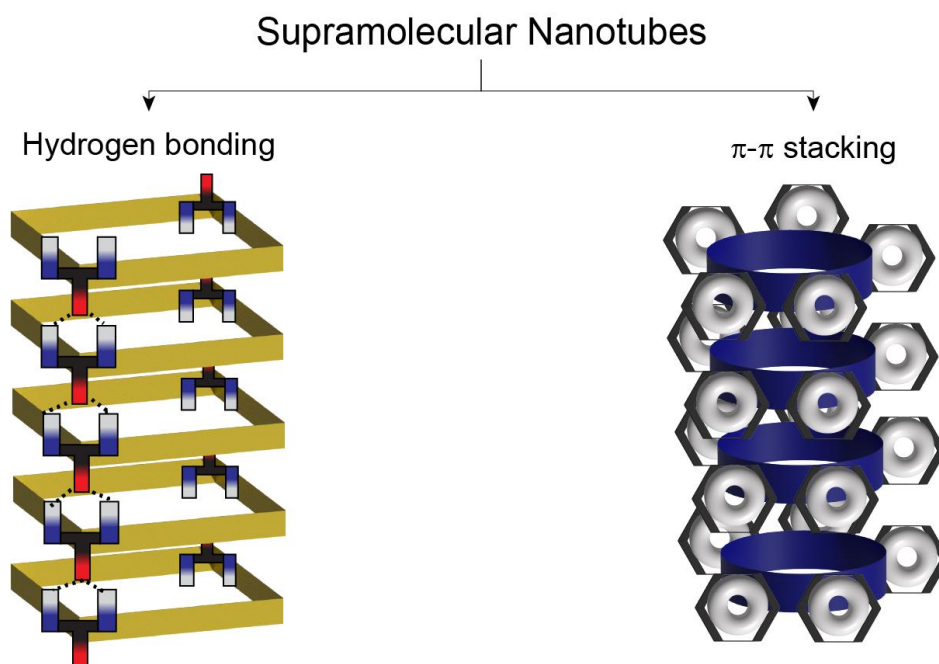
Fig.1.2: Classification of Supramolecular Nanotubes based on Interaction type into Hydrogen-bonding and π-π stacking

In the literature of supramolecular nanotubes, macrocycles, metallocycles or peptides are the most exploited building blocks for monomers. The first described supramolecular nanotube was itself inspired from cyclic peptides by Ghadiri et al. in 1993[11]. This was closely followed by reports of supramolecular nanotubes synthesized from amphiphilic diblock copolymers by Yu and Eisenberg in 1998[12], π-stacked rosette nanotubes by Thiyagarajan et al. in 2002[13] and the first hydrogen-bonded nanotube from macrocycles by Shimizu et al. in 2003[14].

Therefore, the most abundant supramolecular interactions that are exploited in nanotube formation are hydrogen bonding and π-π stacking. Among these,

hydrogen bonding is a directional interaction, and their cohesive nature helps in forming stable yet dynamic supramolecular architectures. π-π stacked tubes, on the other hand, suffer from exfoliation and hence can be considered comparatively less stable. Furthermore, evidence of hydrogen bonding is explicit from single crystal data, and effects can even be indirectly studied using NMR – thus making it easier to prove the existence of supramolecular interactions in nanotubes.

The possible use of small molecules as monomers would considerably reduce the complications associated with the synthesis of supramolecular nanotubes. The directionality of hydrogen bonding combined with molecular geometries can be used to control the dimensionality of the supramolecular assembly, and hence the need to understand the networking capacities of hydrogen-bonded structures has grown over the years.

Hydrogen-bonded organic nanotubes can have various cross-sectional geometries depending on the geometry of the building blocks. A hexagonal nanotube, for example, involves a bent ditopic ligand with a donor and acceptor at each end[15]. Another possible design is that of a rosette nanotube, which combines a hexagonal hydrogen-bonded design with the herringbone structure associated with stacking. Barrelene derivatives are a suitable choice for nanotube building blocks for the possibility of forming extended one-dimensional supramolecular structures. Triptycene is the simplest and most readily available such compound, and hence, our choice of starting material during the course of this thesis.

1.3 Weak Hydrogen Bonds – Detection and Application

Weak hydrogen bonds have been a source of debate in classical literature. However, Steiner and Desiraju have written multiple articles on the modern definition of hydrogen bonds, and its detection from crystallographic and spectroscopic methods. The revised definition of hydrogen bonding given by Pimentel and McClellan in 1960 defines hydrogen bond in terms of electron density by generalizing it to "an already bonded H-atom" having another interaction with a different atom[16]. This definition was thereafter used in a statistical purview with classifications arising with respect to interaction energy, bond length and bond angle cutoffs. Desiraju classified weak hydrogen bonding as interaction having less than 4 kcal/mol energy, bond length between hydrogen and acceptor atom to be greater than 2 Å and the angles can be as low as 90^0[17].
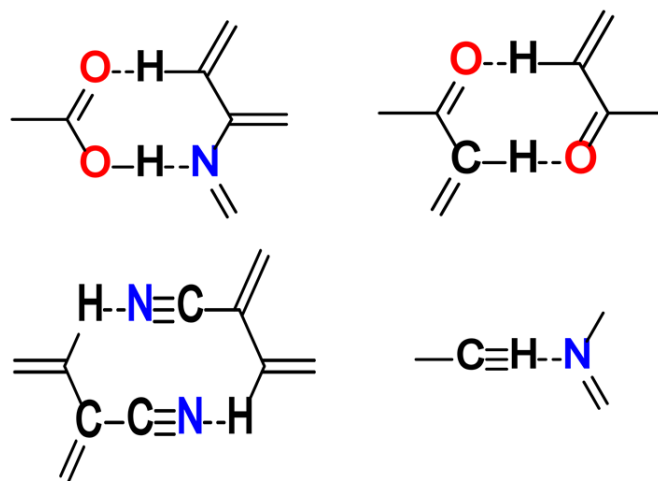
Fig.1.3: Examples of supramolecular synthons based on weak hydrogen bonding

In spite of the low energetics associated with weak hydrogen bonding, it has high utility in crystal engineering. Multiple weak hydrogen bonds often reinforce each other through charge flow or mutual polarization, hence resulting in additional stability than individual hydrogen bonds[18]. This cooperativity plays a key role in stabilizing supramolecular macromolecules in the dimension of the hydrogen bonding chain. Thus, there are a lot of supramolecular synthons based on weak hydrogen bonding[19]. Even in the case of one-dimensional nanotubes, Fabiola's analysis of hydrogen bond geometries in peptides shows that the concerted nature of the C-H⋯O-C(ketone) bonds plays a massive significance in not forming β-sheets, even though each of them are energetically only around 1 kcal/mol[20]. Weak hydrogen bonds like C-H⋯O are also able to differentiate between alternative strong hydrogen bond networks in a crystal structure, thus effectively choosing a crystallization pathway from numerous possibilities.

Weak hydrogen bonding provides a unique blend of stability and flexibility in supramolecular architectures, which has therefore seen applications in molecular recognition and polymer catalysis. In a recent article by Parra, it is shown *via* DFT that C-H⋯O bonding was the driving force behind the nanotube formation from a bolaamphiphile[21]. The application of weak hydrogen bonding in recognition is also extensively discussed by Zehnecker[22] and Roelens[23].

1.4 Scope of the thesis

This thesis explores a new design for one-dimensional hydrogen-bonded nanotubes with a tetragonal cross-section. We perform a bottom-up synthesis of the building block, thus overcoming the difficulties of synthesizing large macrocycles or peptide derivatives. Recently, Banerjee et al. published a covalent organic nanotube based on tetraamino triptycene and terephthaldehyde[24]. We wanted to observe whether we could develop a supramolecular nanotube from a similar motif by mimicking the design from biological transport systems.

Furt+hermore, the appearance of weak hydrogen bonds in the crystal structure piqued our interest. Hence, we crystallized the monomer in different solvents and were able to obtain polymorphs based on the magnitude of interaction with the solvent – most of which involved hydrogen bonding. Although the backbone of the design is based on strong hydrogen bonds in between imidazole moieties, the solvent stabilization played a crucial role in the optimal crystallization route in each case.

Moreover, to the best of our knowledge, a computational DFT study of polymorphism in supramolecular structures is unprecedented. Therefore, we aimed to provide a comprehensive understanding of the driving forces behind nanotube formation in our system.

Experimental Methods

2.1 Synthesis

Materials: All reactions were performed under inert conditions (nitrogen or argon atmosphere) in standard borosilicate glassware. Solvents were purchased locally and used without further purification. Triptycene was purchased from BLD Pharma and used as received. All other reagents were bought from Sigma Aldrich and used without modification.

Nuclear Magnetic Resonance Spectroscopy (NMR): NMR spectra of all compounds were recorded on a Bruker 400 MHz spectrometer (^{1}H NMR: 400 MHz) at room temperature using TMS as an internal reference. Deuterated solvents were purchased from BLD Pharma and used as received.

Fourier Transform Infrared (FT-IR) Spectra: The FT-IR spectrum was recorded on a Bruker Optics ALPHA II spectrometer with a universal Zn-Se ATR (attenuated total reflection) accessory.

Single crystal X-ray diffraction (SC-XRD): All single crystal data has been collected in XtaLAB Synergy, Dualflex, HyPix3000 diffractometer using Cu-Kα = 1.54184 Å radiation at 100 K for TAT and TAT-Im in DMF, and using Mo- Kα = 0.71073 Å for TAT-Im in DCM. The X-ray data acquisition was supervised by the Olex-2.0 program suit[25]. Using Olex2, the structure was solved with the olex2.solve structure solution program using Charge Flipping and refined with the olex2.refine refinement package using Gauss-Newton minimisation. Mercury software was utilized for molecular representations and packing diagrams[26]. The refinement of anisotropic thermal parameters of non-hydrogen atoms was done with the full-matrix least-squares method.

2.1.1 Dinitrotriptycene
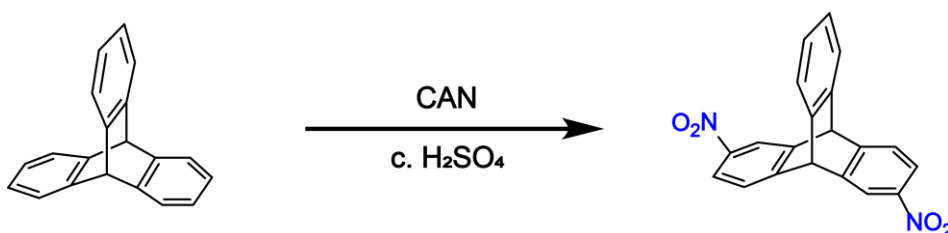
Scheme. 1: Synthesis of dinitrotriptycene

Synthesis was done using previously reported procedure.[27] To a 250 mL round-bottom flask equipped with a magnetic stir bar is added 5 g (20 mmol) of triptycene and solubilized in 100 mL DCM. 22 g (40 mmol) CAN and 4 mL (36 mmol) of conc. sulphuric acid is added to the reaction mixture and stirred at room temperature for 12 hours. The reaction mixture changes color from orange to dark green over this time period. The resulting solution is filtered to remove the cerium salts, and the filter cake is washed with DCM as long as the filtrate is UV-active on TLC. The combined

filtrate is neutralized using 200 mL of 10% potassium carbonate (aq.). The organic layer is separated and the aqueous phase is extracted with more DCM (2 X 100 mL). The collective organic layers are dried using anhydrous sodium sulfate, and the solvent is removed under reduced pressure via rotavapor. Finally, the residue is purified via column chromatography (eluent 15-25% v/v DCM/Hexane) to give a mixture of *2,6-* and *2,7-* Dinitrotriptycene as a pale yellow powder.

2.1.2 Diacetamidodinitrotriptycene
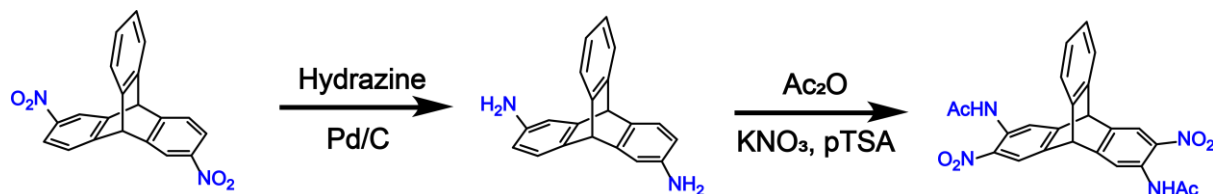
Scheme. 2: Synthesis of diacetamidodinitrotriptycene

To an ice-cooled solution (0ºC) of 100 mL ethanol is added 3.44 g (10 mmol) of both isomers of Dinitrotriptycene, followed by 340 mg of 10 wt% Pd/C and 3.4 mL of hydrazine monohydrate. The reaction mixture is stirred at reflux overnight and then cooled to room temperature. The resulting solution is filtered through a Celite pad and the filter cake is washed with 60 mL ethanol. The filtrate is then evaporated in rotavapor to give *2,6-* and *2,7-* Diaminotriptycene as an off-white solid.

The obtained Diaminotriptycene is added to 100 mL acetic anhydride and stirred for around 90 minutes at room temperature. 4.19 g (22 mmol) of para-Toluene sulphonic acid is used to solubilize the contents of the reaction mixture and then 2.12 g (21 mmol) of potassium nitrate is added. The resulting solution is stirred overnight at room temperature, added to 500 mL water and further stirred for an hour. Then the solution is filtered, and the filter cake is washed with water (3 X 50 mL) to give a yellow-orange residue. The residue is dissolved in 150 mL DCM, dried with sodium sulfate and then the solvent is removed at reduced pressure via rotavapor. The resulting solid is purified via column chromatography (eluent DCM) to give a mixture of syn- and anti- Diacetamidodinitro triptycene as a pale yellow powder.

2.1.3 Diaminodinitrotriptycene
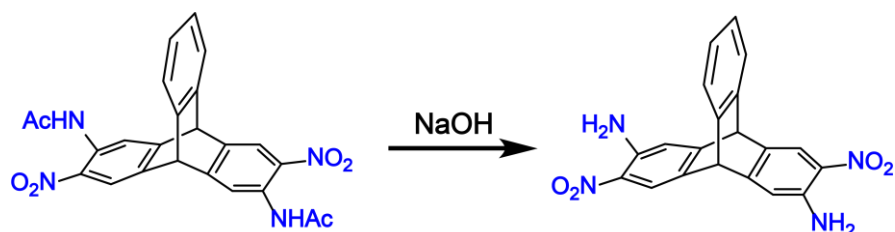
Scheme. 3: Synthesis of diaminodinitrotriptycene

1.2 g (30 mmol) of NaOH is dissolved in 3 mL water via sonication. 1.37 g (3 mmol) of the mixture of both isomers of Diacetamidodinitro triptycene is added to a 100 mL round-bottom flask fitted with a magnetic stir bar and solubilized in 30 mL ethanol. The aqueous NaOH solution is added to the flask and the reaction mixture is stirred under reflux for 3 to 4 hours. The solution was evaporated under reduced pressure

via rotavapor and the residue was suspended in 60 mL water, filtered and further washed with water (3 X 10 mL) and methanol (2 X 10 mL) to give syn- and anti-Diaminodinitrotriptycene as a dark orange solid.

2.1.4 Tetraaminotriptycene
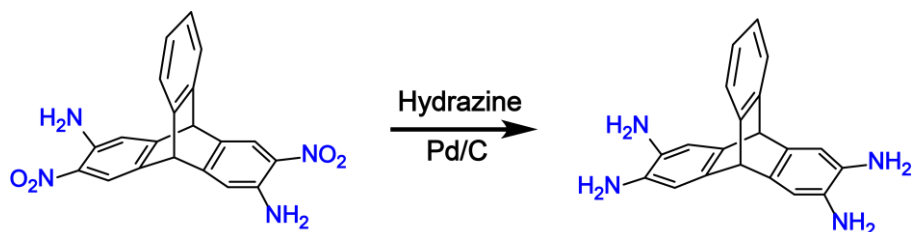
Scheme. 4: Synthesis of tetraaminotriptycene

To an ice-cooled solution (0ºC) of 30 mL ethanol is added 374 mg (1 mmol) of Diaminodinitro triptycene, followed by 58 mg of 10 wt% Pd/C and 1 mL of hydrazine monohydrate. The mixture is refluxed overnight and then cooled to room temperature. The reaction mixture is then filtered through a Celite pad and the filter cake is washed with boiling methanol (3 X 100 mL). The filtrate is then refrigerated for 12 hours, and crystals of tetraamino triptycene are precipitated. The crystals are then isolated by filtration and dried overnight in vacuo to give Tetraamino triptycene as fluffy off-white crystal chunks.

2.1.5 TAT-Im
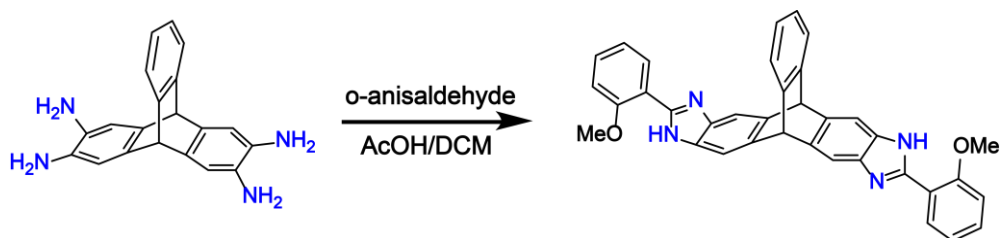
Scheme. 5: Synthesis of TAT-Im

31.5 mg (0.1 mmol) TAT has been taken in a 100 ml round bottom flask and dissolved in 50 ml dichloromethane. 27.2 mg (0.2 mmol) o-anisaldehyde is added into the clear solution in the presence of a catalytic amount (100 µL) of glacial acetic acid. The whole mixture is then kept under reflux for two days. After completion of the reaction, the DCM was evaporated, and the TAT-Im compound was isolated after purification with column chromatography (DCM as eluent).

TAT-Im was later recrystallized in DCM via slow evaporation for 6 hours and in DMF via heating at 120ºC for seven days.

2.2 Density Functional Theory (DFT) calculations

General Theory:

Density-functional theory (DFT) is one of the most widely used computational methods used to model systems from a quantum mechanical perspective, for example, to understand the energy states of materials and to predict spectroscopic properties. Computational runtime for DFT is relatively low when compared to methods like Hartree–Fock theory and hence their extensive use.

The method involves the use of functionals representing spatially dependent electron density. By calculating the potential from the functionals, we are able to understand the components arising from the elemental composition of the system as well as from the interactions between them. Thus, an n-electron problem is effectively reduced to the study of n interdependent one-electron equations, called Kohn–Sham equations[28].

These equations are further simplified by considering realistic assumptions, such as the local-density approximation (LDA), where the functional depends only on the electron density at the point of evaluation. In calculations for crystal systems, one often couples LDA with plane wave basis sets to represent delocalization through an infinite solid.

One popular functional is known as BLYP, for which the exchange part was proposed by Becke[29] while Lee, Yang and Parr are credited for the correlation part[30]. B3LYP is a hybrid functional based on BLYP where the exchange energy is matched with Hartree–Fock theory energy values[31]. The advantage of using a hybrid functional like B3LYP is the presence of three additional parameters which determine the amount of mixing of basis sets, resulting in higher refinement precision. The parameters are also fine-tuned using a training set consisting of a wide range of molecules, resulting in more effective calculations.

For solution state DFT, there are a range of solvation models available. The most widely used is the polarizable continuum model (PCM), where the solvent is treated as a uniform electron density cloud surrounding the solute envelope[32]. In all PCM models, solute charge density is assumed to be enclosed within a cavity. However, the Integral Equation Formalism Polarizable Continuum Model (IEFPCM) is shown to be the most flexible model to account for the delocalization of solute charge density outside the cavity, and hence we chose that model for our calculations[33].

Procedure:

To further understand the role of solvents in the polymorphism of TAT-Im, we decided to perform DFT calculations. All DFT calculations were performed using Gaussian09 software[34]. The crystal structure of TAT-Im in DCM was used to build the initial structure, and other solvent molecules were inserted in place of DCM with random orientations. Geometry optimization was then performed using Avogadro before submitting to Gaussian09 via Gaussview platform.

All calculations involved using the B3LYP functional, and the basis sets used were 6-31g(d) for carbon, nitrogen, oxygen and chlorine atoms; 6-31g for hydrogen atoms and Lanl2dz for sulfur atoms. Solution state DFT for monomers was done using the IEFPCM model, while for polymeric states individual solvent molecules were introduced following the crystal structure of TAT-Im in DCM. The eight solvents chosen to run the calculations on are DMF, DMSO, ethyl acetate, DCM, chloroform, carbon tetrachloride, THF and acetonitrile due to the moderate to high solubility of TAT-Im in these solvents.

Chapter 3

Results and Discussion

3.1 Characterization of intermediates

3.1.1 Dinitrotriptycene

During the synthesis of dinitrotriptycene, mononitrotriptycene was obtained as a by-product. It was isolated during column chromatography and characterized using NMR spectroscopy as shown below.
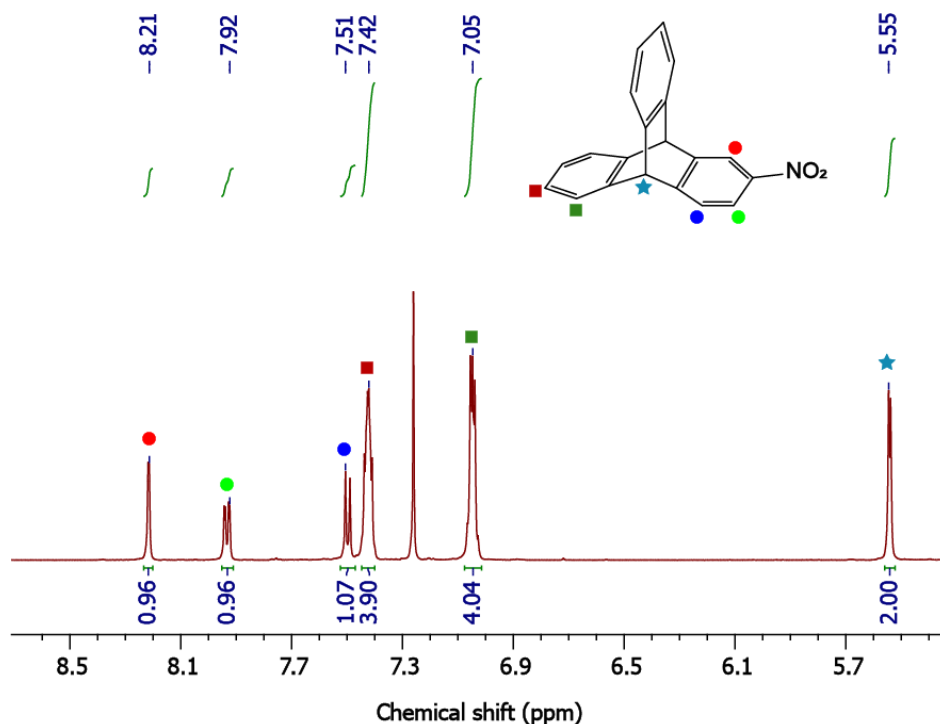
Fig.3.1: ^{1}H NMR of Mononitrotriptycene: ^{1}H NMR (500 MHz, CDCl$_3$) δ 8.21 (d, 1H), 7.93 (dd, J = 8.1, 2.3 Hz, 1H), 7.50 (d, J = 8.1 Hz, 1H), 7.42 (m, 4H), 7.05 (m, 4H), 5.54 (d, J = 3.7 Hz, 2H).

On the other hand, the NMR spectra of dinitrotriptycene showed some interesting properties. Two possible isomers of dinitrotriptycene can be formed – 2,6- or the syn isomer, and 2,7- or the anti isomer. We obtain three peaks for the bridgehead proton H$_f$ in the range of 6.14-6.20, which can be attributed to the presence of both syn- and anti- forms of the compound, with two peaks belonging to the syn form and one peak belonging to the anti form. Nitration of aromatic compounds generally occurs by S$_N$Ar mechanism, and in this case as well there is no exception as we observe no significant selectivity of one isomer over the other.

The other aromatic peaks also show apparent higher-order splitting patterns than expected due to the product being isolated as a mixture of isomers. For example, the proton H$_e$ which seems to show a doublet of doublet, is actually two doublets obtained from the syn and anti forms, each arising possibly due to meta coupling.

Isolation of a single isomer was possible with careful chromatography as reported in the literature, however since the final product is identical we used the obtained mixture itself for further reactions.
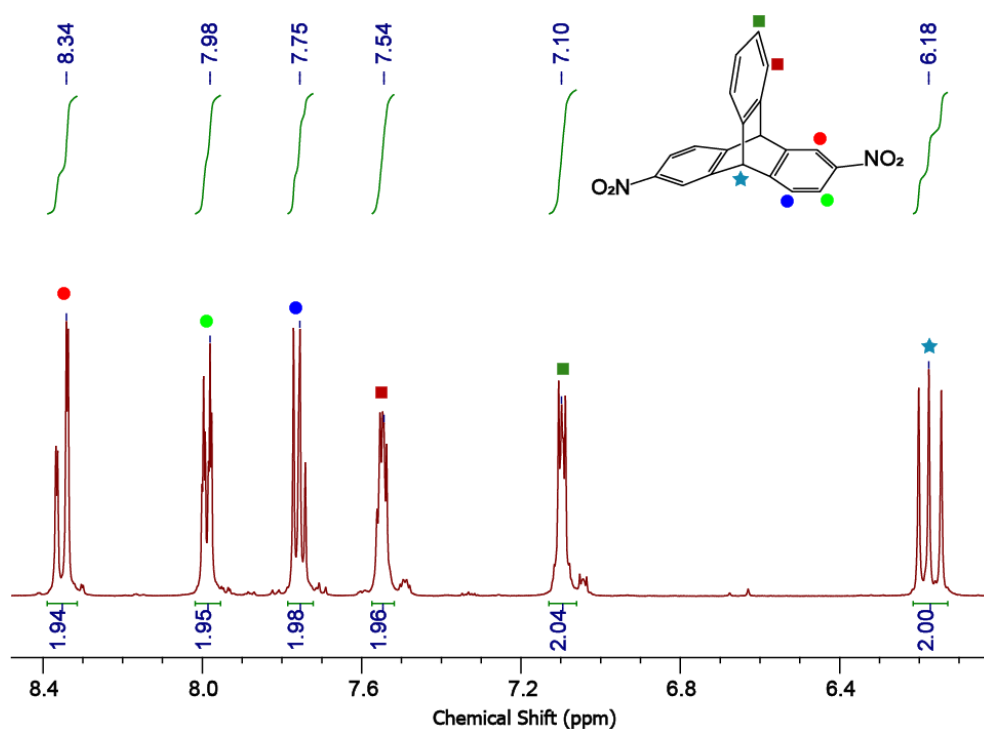
Fig.3.2: ¹H NMR of both isomers of Dinitrotriptycene: ^{1}H NMR (500 MHz, DMSO) δ 8.35 (dd, J = 13.2, 2.3 Hz, 2H), 7.99 (dt, J = 8.1, 2.1 Hz, 2H), 7.76 (dd, J = 8.2, 6.6 Hz, 2H), 7.56 – 7.54 (m, 2H), 7.11 – 7.09 (m, 2H), 6.20 – 6.14 (m, 2H).

3.1.2 Diacetamidodinitrotriptycene
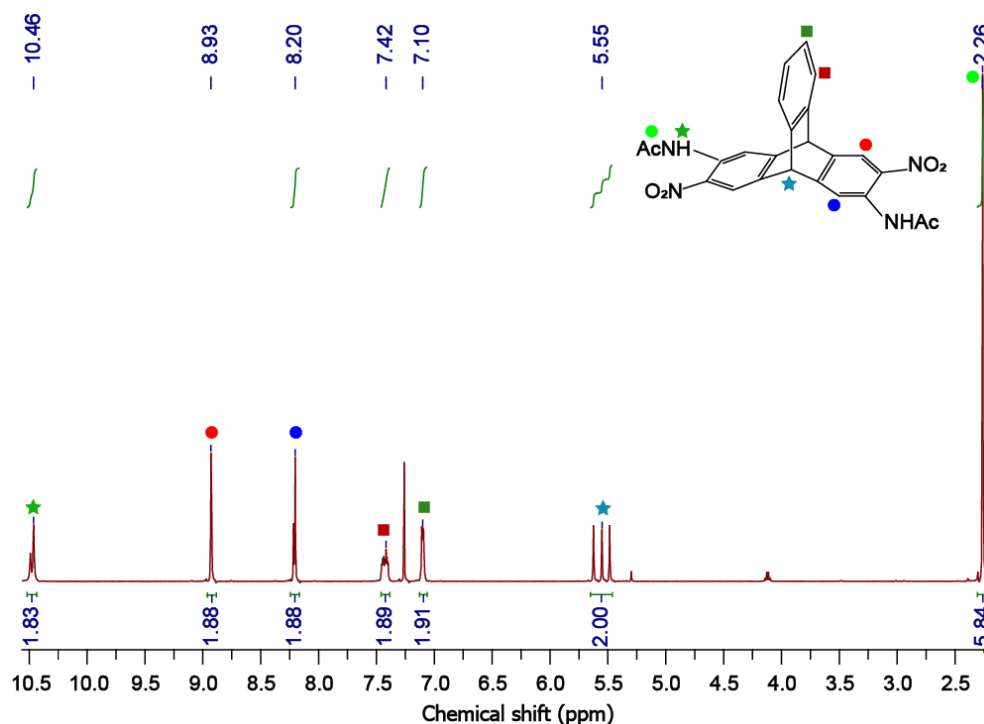
Fig.3.3: ¹H NMR of both isomers of Diacetamidodinitro triptycene: ^{1}H NMR (500 MHz, CDCl₃) δ 10.48 (d, J = 14.1 Hz, 2H), 8.93 (d, J = 3.5 Hz, 2H), 8.21 (d, J = 6.6

23

Hz, 2H), 7.42 – 7.38 (m, 2H), 7.10 (dd, *J* = 5.4, 3.2 Hz, 2H), 5.62-5.48 (m, 2H), 2.26 (s, 6H).

The synthesis of diacetamidodinitrotriptycene from dinitrotriptycene involves two steps of reduction and protection. However, since both these processes involve excess reagents and reaction times, we are able to directly obtain the acetamido product without any complicated purification techniques. In this compound as well, we see the signature NMR peak of the bridgehead protons showing a pseudo "triplet" arising from the possibilities of syn- and anti- conformations. Additionally, the sharp peak of the acetyl protons is seen at 2.26 ppm.

3.1.3 Dinitrodiaminotriptycene
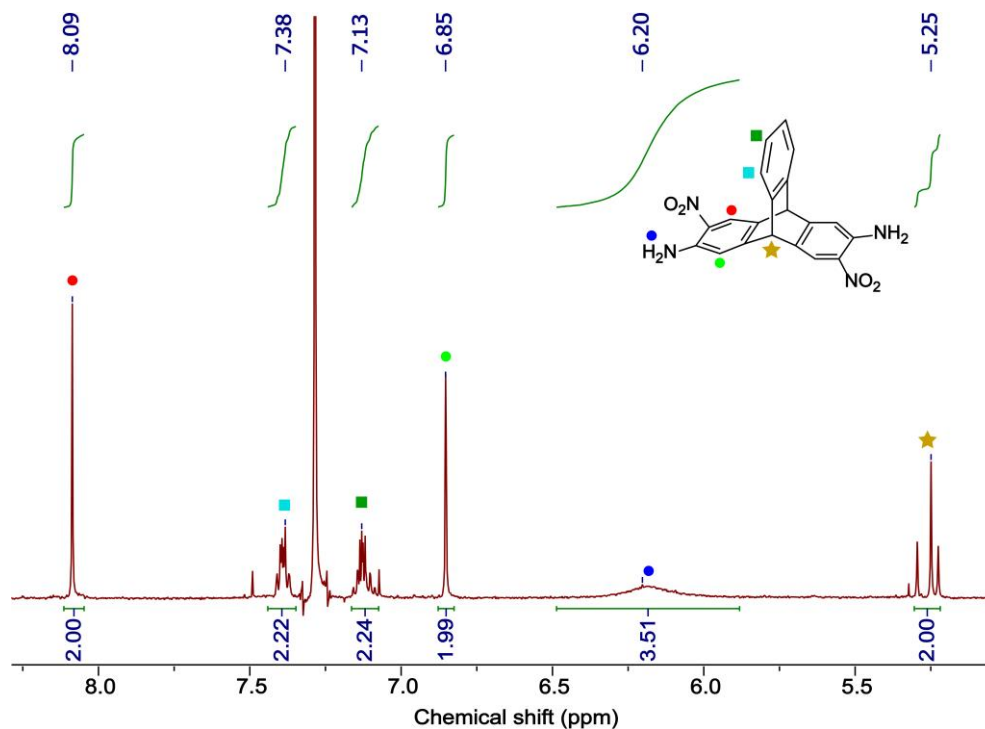
Fig.3.4: ^{1}H NMR of both isomers of Diaminodinitro triptycene: ^{1}H NMR (500 MHz, CDCl₃) δ 8.09 (s, 2H), 7.43-7.39 (m, 2H), 7.18 – 7.10 (m, 2H), 6.85 (s, 2H), 6.40-6.00 (m, 4H), 5.29-5.23 (m, 2H).

The deprotection of diacetamidodinitrotriptycene by NaOH is again a simple step where using excess NaOH leads to the isolation of product simply through the basic work-up procedure. A key feature of the NMR spectra is the broad peak around 6.2 ppm wich is indicative of the amine group. The broadening is due to the fast exchange of the labile amine protons in chloroform-d. We also again see the bridgehead peaks, and we are able to identify the ratio of syn- and anti- product formed.

3.1.4 Tetraaminotriptycene

The NMR spectrum of tetraaminotriptycene (TAT) is highly distinctive and has four singlet peaks. The high purity of the crystals is reflected in the sharpness of the peaks. The bridgehead protons occur at 4.88 and is no longer a triplet because TAT only has one isomer. Furthermore, the NMR spectrum is taken in DMSO-d₆ due to

the low solubility in chloroform. This also results in a narrow amine peak at 4.13 because the exchange rate of the amine protons is drastically slowed down in DMSO.
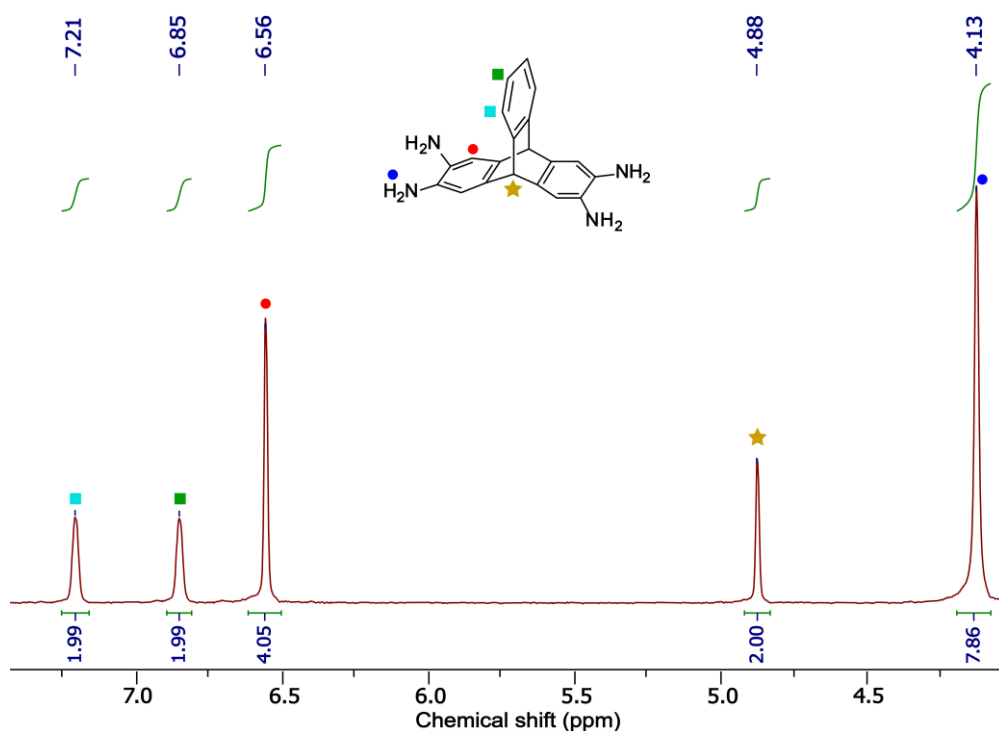
Fig.3.5: ^{1}H NMR of both isomers of Tetraamino triptycene: ^{1}H NMR (500 MHz, DMSO) δ 7.24 – 7.19 (m, 2H), 6.88 – 6.83 (m, 2H), 6.56 (d, *J* = 3.2 Hz, 4H), 4.88 (s, 2H), 4.13 (s, 8H).

The IR spectrum of TAT also shows some characteristic peaks – the broad N-H stretching frequency around 3100-3300 cm^{-1}, and the aromatic C-C stretching frequency around 1500-1600 cm^{-1}.
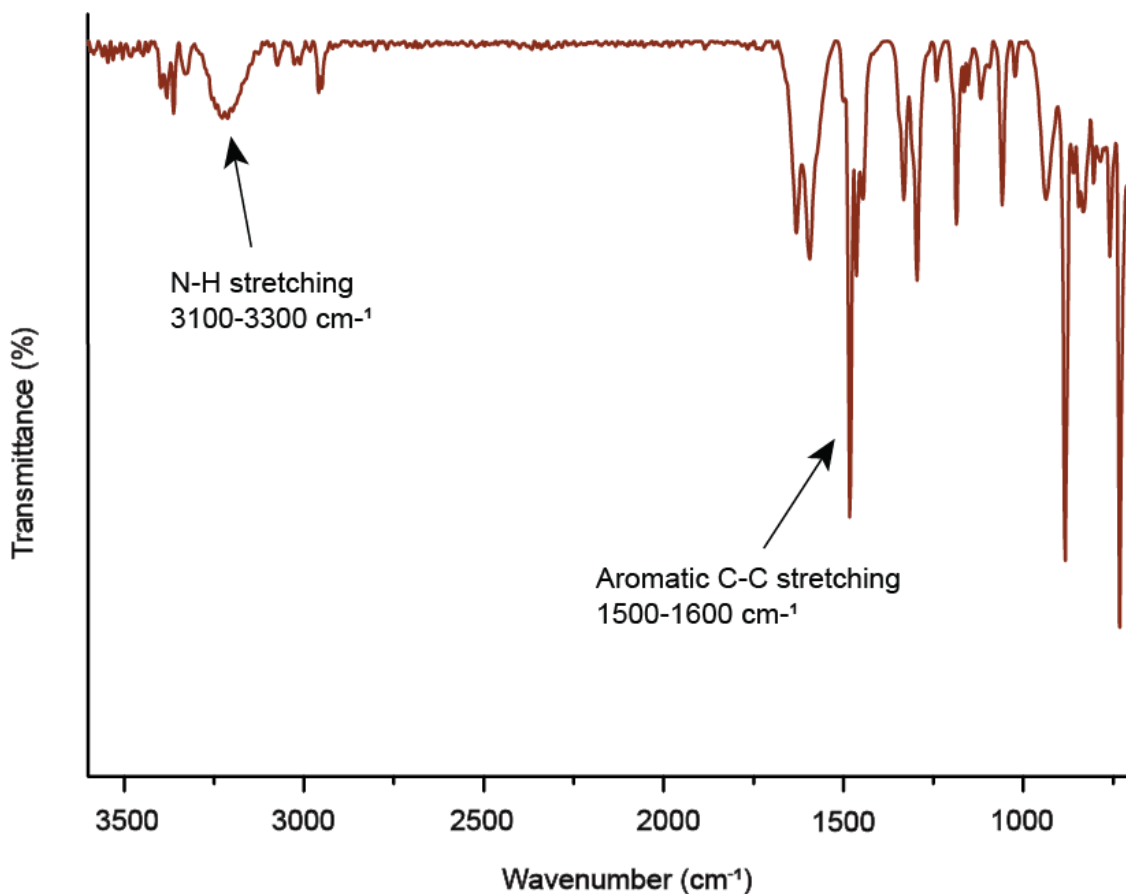
Fig.3.6: IR spectrum of Tetraamino triptycene: N-H stretching peak of amine group between 3100-3300 cm^{-1}, aromatic C-C stretching peak between 1500-1600 cm^{-1}

a)

b)
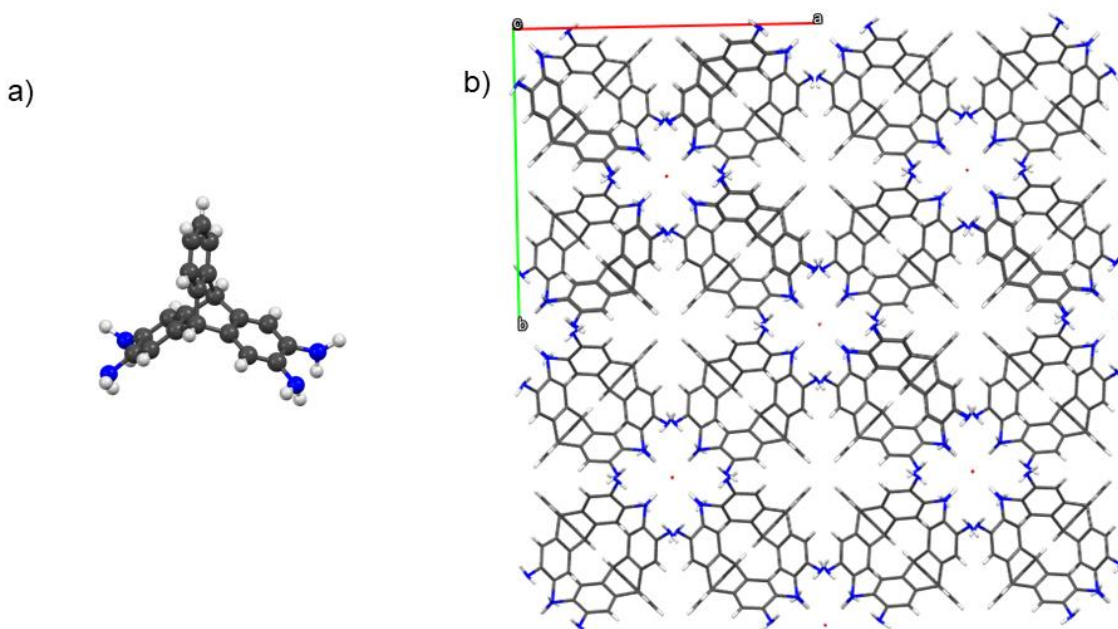
Fig.3.7: a) The single crystal structure of Tetraamino triptycene (TAT)

b) The crystal packing of TAT

Finally, the single crystal data of off-white fluffy TAT crystals was collected at 100 K and showed the tetragonal space group of $I4cm$. The unit cell accommodates 8 TAT molecules – 4 TAT molecules arranged in fourfold symmetry around the OH^- of methanol solvent at the center. OH^- forms a body-centred lattice and the TAT molecules are packed with hydrogen bonding playing a major role in the packing.

Property	Value
Structural formula	0.5(O), $C_{20}H_{18}N_4$
Formula weight	322.38
Crystal system	Tetragonal
Space group	$I4cm$
T (K)	100.0(2)
a (Å)	19.6402(6)
b (Å)	19.6402(6)
c (Å)	8.2350(3)
α (º)	90
β (º)	90
γ (º)	90
V (Å^3)	3176.5(2)
Z	8
ρ (calc.) (g cm^{-3})	1.348
μ (mm^{-1})	0.668
R$_{int}$	0.0330
R$_1$ [I>2σ(I)]	0.0728
wR$_2$	0.1776
Goodness-of-fit on F^2	1.158

Reflections collected	6152
Unique reflections	1250
largest diff peak and hole (e Å^{-3})	0.36/-0.30

Table 3.1: Property table for single crystal data of Tetraamino triptycene

There are three different types of hydrogen bonds we see in the crystal structure of TAT. Each TAT molecule forms a strong N-H...O hydrogen bond with the OH$^-$, with the donor-acceptor distance being just over 2 Å and an almost linear angle of 168°. Four of these hydrogen bonds are formed with the same solvent O. Alongside, we have two distinct N-H...N bonds between the TAT molecules. Each TAT molecule forms two shorter and angular N2-H...N5 type bonds with TAT molecules sharing a N-H...O...H-N synthon, and also forms a longer and straighter N5-H...N2 bond with the TAT molecule located along the c-glide.

This crystal structure gives us an idea of the possibility of the formation of tetragonal nanotubes through the use of triptycene derivatives.

Hydrogen bond	**D (Å)**	**d (Å)**	**Angle (°)**
N-H...2	3.035(9)	2.36	128
N-H...N	3.544(9)	2.66	174
N-H...O	3.199(9)	2.12	169

Table 3.2: Hydrogen bond distances and angles in Tetraamino triptycene

3.1.5 TAT-Im
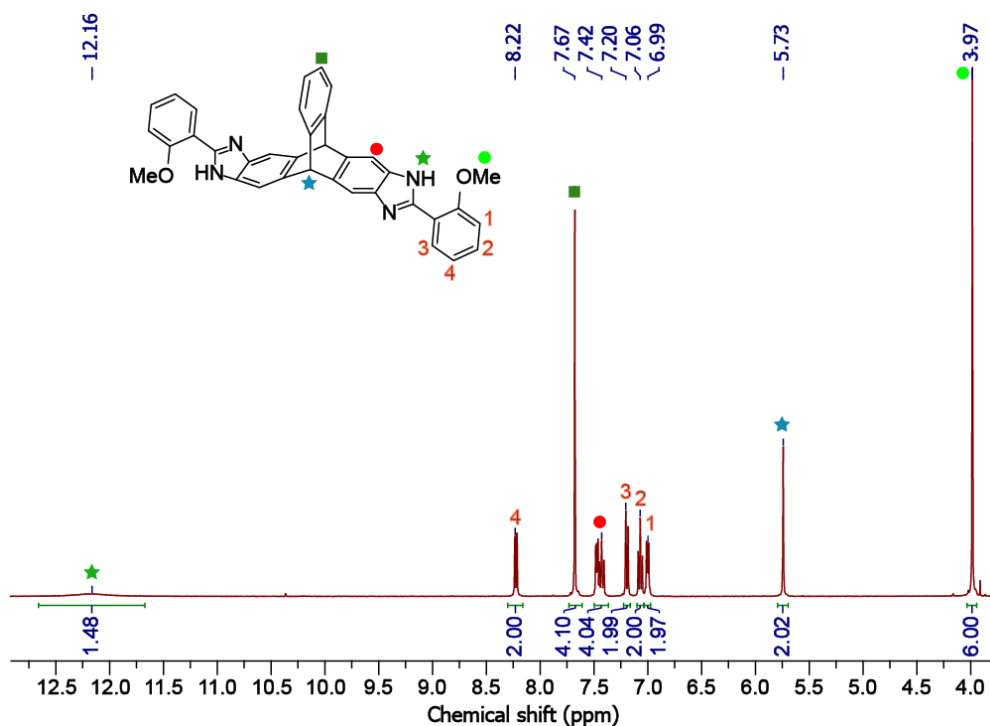
Fig.3.8: ^{1}H NMR of TAT-Im: ^{1}H NMR (400 MHz, DMSO-D_6) δ 12.17 (s, 2H), 8.22 (s, 2H), 7.67 (s, 4H), 7.48 (s, 4H), 7.17 (s, 2H), 7.06 (s, 2H), 6.99 (s, 2H), 5.73 (s, 2H), 3.98 (s, 6H).

The NMR spectrum of TAT-Im has a lot of complicated peaks in the aromatic region due to the presence of two unique rings. Nevertheless, the peak around 12.1 ppm is well known to belong to the imidazole moiety, and with careful assignment of the remaining peaks we are able to confirm the formation of TAT-Im.

3.2 Solvent-dependent crystallization of TAT-Im

3.2.1 Crystallization in DCM
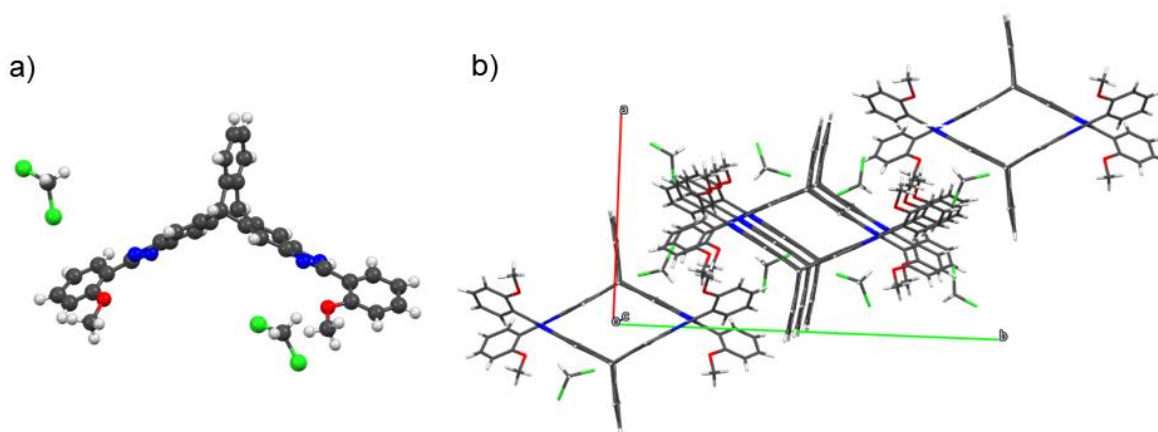
Fig.3.9: a) The single crystal structure of TAT-Im in DCM (asymmetric unit)

b) The crystal packing of TAT-Im in DCM showing parallel nanotubes

Property	Value
Structural formula	CH_2Cl_2, $0.5(C_{36}H_{26}N_4O_2)$
Formula weight	358.249
Crystal system	Orthorhombic
Space group	$Pna2_1$
T (K)	102.15
a (Å)	13.6629(5)
b (Å)	25.0200(9)
c (Å)	10.1345(4)
α (º)	90
β (º)	90
γ (º)	90
V (Å^3)	3464.4(2)
Z	8
ρ (calc.) (g cm^{-3})	1.374
μ (mm^{-1})	0.382
R_{int}	0.0473
R_1 [I>2σ(I)]	0.1346
wR_2	0.3690
Goodness-of-fit on F^2	1.041
Reflections collected	26975
Unique reflections	7139
Largest diff peak and hole (e Å^{-3})	1.90/-0.91

Table 3.3: Property table for single crystal data of TAT-Im in DCM

The solution of TAT-Im in DCM under slow evaporation over 6-8 hours produced long needle-like crystals. From single crystal XRD data, we observe that the crystallization occurred in the orthorhombic space group of *Pna2₁*. Furthermore, we notice the helical structure growth along the b-axis giving rise to a nanotubular structure.

On further inspection, we find that there are a number of dissimilar hydrogen bonds that are responsible for supporting this supramolecular structure. Firstly, the strong N-H...N bond forms the backbone of the nanotube with a distance of only around 2 Angstroms. However, there are four more weak hydrogen bond interactions that lend stability – two of them being well-reported C-H...O interactions and a couple of rare C-H...Cl interactions.

There is one interaction between the oxygen in the methoxy group of TAT-Im with the C-H of solvent, and another interaction with one C-H of the phenyl ring of the adjacent TAT-Im. The C-H...O bond with the solvent is shorter, however it is bent due to the oxygen atom participating in a bifurcated hydrogen bond with both the solvent and the phenyl ring.

C-H...Cl bonds are highly debated in literature, however in this case, we discern that the C-H...Cl interactions satisfy both the geometric cutoffs for weak hydrogen bonds as laid out by Steiner and Desiraju. Both the C-H...Cl interactions have lengths of less than 3 Å and angles larger than 140⁰. Hence, we are able to classify them as weak hydrogen bonds and explore their utility by computational means as shown later.

Hydrogen bond	D (Å)	d (Å)	Angle (⁰)
C-H...O	3.22(3)	2.52	127
N-H...O	3.237(15)	2.71	119
C-H...O	3.616(16)	2.67	171
C-H...O	3.625(18)	2.71	163
C-H...Cl	3.838(11)	2.96	155
C-H...Cl	3.743(13)	2.83	161
C-H...Cl	3.774(18)	2.91	148
N-H...N	2.824(16)	1.99	158
N-H...N	2.880(17)	2.08	151

Table 3.4: Hydrogen bond distances and angles for TAT-Im crystal in DCM

3.2.2 Crystallization in DMF

The solution of TAT-Im in DMF was kept in a 120ºC oven for 7-10 days to get small white crystals. From single crystal XRD data, we observe that the crystallization occurred in the triclinic space group of $P\bar{1}$, indicating a loss of symmetry compared to the crystal in DCM. Additionally, no one-dimensional superstructure is observed, we notice cross-linked TAT-Im dimers formed instead with DMF blocking the crystal growth sites.

The N-H...N and C-H...O were of similar length as that of the polymorph formed in DCM, however there was an additional N-H...O hydrogen bond formed between the imidazole and DMF at two ends of the dimer. The geometric parameters indicated that this N-H...O hydrogen bond was strong – with a length of 2.1 Å and an angle around 140º. Hence we hypothesized that these strong interactions with the solvent prevented the formation of one-dimensional nanotubes. However, we were unable to crystallize in other solvent systems, so we took to computational means to understand the energetics and kinetics behind nanotube formation as shown in section 3.3.
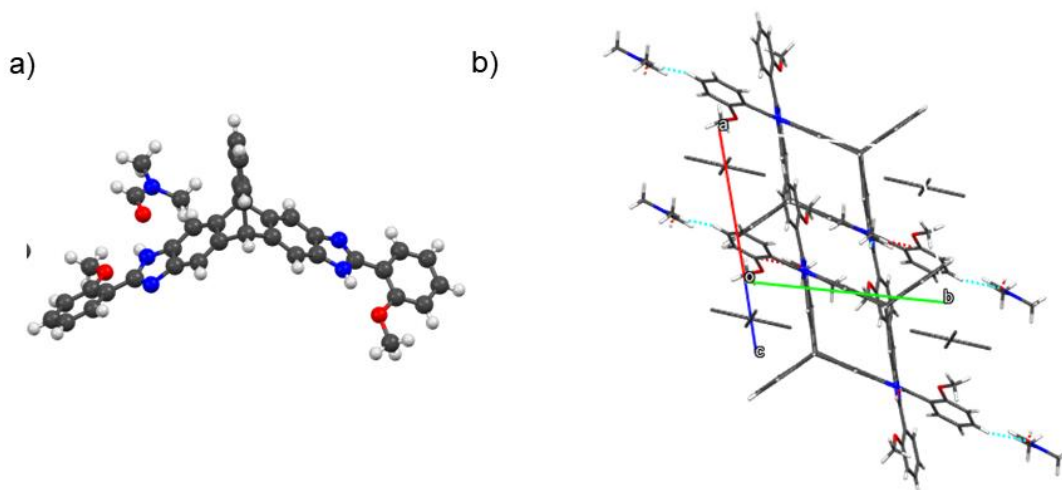
Fig.3.10: a) The single crystal structure of TAT-Im in DMF (asymmetric unit)

    b) The crystal packing of TAT-Im in DCM showing DMF blocking growth sites

Property	Value
Structural formula	$C_{36}H_{26}N_4O_2$, C_3H_7NO
Formula weight	619.26
Crystal system	Triclinic
Space group	$P\text{-}1$

T (K)	102(3)
a (Å)	12.1120(2)
b (Å)	12.9113(2)
c (Å)	13.1944(2)
α (º)	61.402(2)
β (º)	67.1670(10)
γ (º)	83.9900(10)
V (Å^3)	1661.28(5)
Z	2
ρ (calc.) (g cm^{-3})	1.333
μ (mm^{-1})	0.707
R_{int}	0.0591
R_1 [I>2σ(I)]	0.0515
wR_2	0.1393
Goodness-of-fit on F^2	1.028
Reflections collected	30092
Unique reflections	6021
Largest diff peak and hole (e Å^{-3})	0.78/-0.59

Table 3.5: Property table for single crystal data of TAT-Im in DMF

Hydrogen bond	**D (Å)**	**d (Å)**	**Angle (º)**
N-H...O	2.634(2)	2.10	119
N-H...O	2.705(2)	2.27	111
C-H...O	3.449(3)	2.56	155

N-H...O	2.860(2)	2.11	143
N-H...N	2.955(2)	2.12	159

Table 3.6: Hydrogen bond distances and angles for TAT-Im crystal in DMF

3.3 Computational Analysis

We wanted to understand the effects of solvent on nanotube formation and crystallization. In this regard, there are three parameters that come to mind – the relative solvation energy, the stabilization energy for formation of dimer crystal from monomer solution and the stabilization energy for polymer formation from monomer solution. Only an optimal value for each of these parameters would lead to the formation of a one-dimensional superstructure.

3.3.1 Solution state calculations for TAT-Im monomer

We started out by calculating the solvation energies of TAT-Im monomer in different solvents. This was calculated as follows:

Solvation energy (E_{01}) = Energy in solution (E_1) – Isolated energy (E_0)

Solvent	Dipole moment (D)	Solvation energy (kcal/mol)	Relative solvation energy w.r.t DCM (kcal/mol)
None	0	0	+15.15
Carbon tetrachloride	0.0005	-7.03	+8.11
Chloroform	1.6494	-12.20	+2.95
Ethyl acetate	1.9048	-13.46	+1.69
DCM	2.3091	-15.15	0
THF	2.3182	-14.43	+0.72
DMF	3.0358	-18.20	-3.05
Acetonitrile	3.9346	-18.15	-3.00
DMSO	4.6829	-18.42	-3.27

Table 3.7: DFT calculated dipole moment and solvation energy of TAT-Im in different solvents
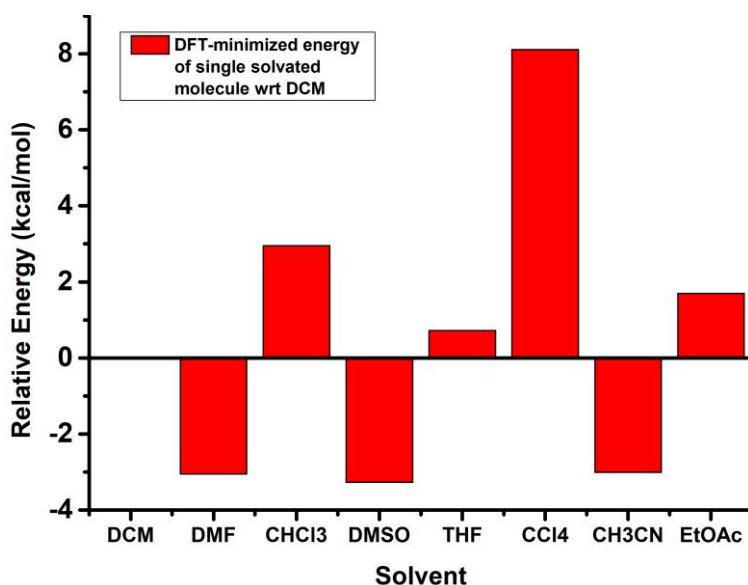

Fig.3.11: Relative solvation energy of TAT-Im monomer in different solvents

It is clearly observed that TAT-Im showed large solvation energy in solvents where there is a change of large solute-solvent interaction through hydrogen bonds. The highest solvation energies occur with DMF, acetonitrile and DMSO – all of which have a hydrogen bond acceptor atom in the form of N or O.
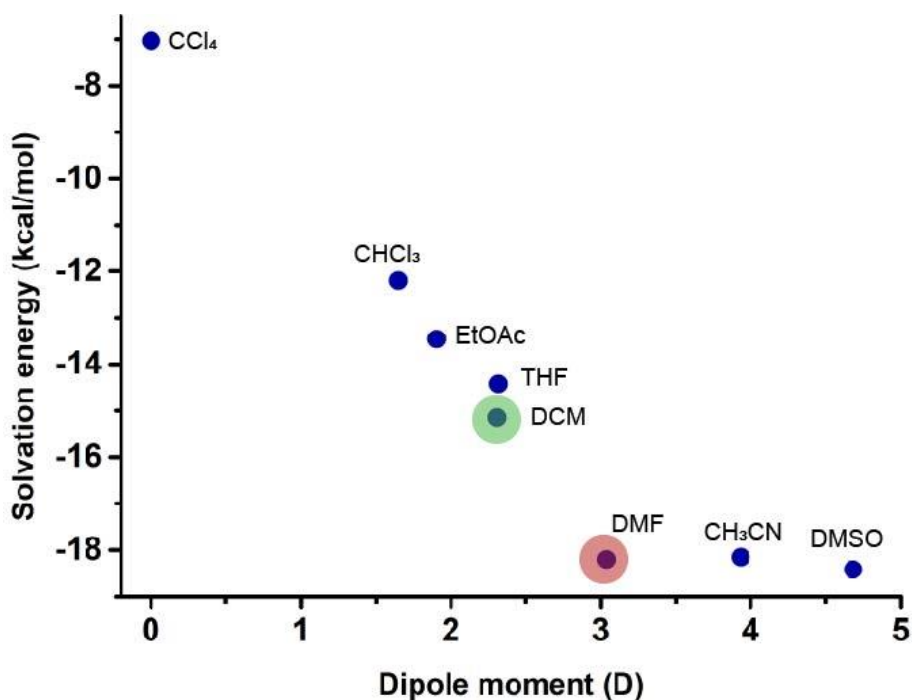

Fig.3.12: Correlation plot between solvation energy and dipole moment of solvents

We further correlated the solvation energy with DFT calculated dipole moments of the solvents, and observed a definite negative correlation. Hence we inferred that more polar solvents would offer high stability to TAT-Im in solution, and thus would be difficult to crystallize into a nanotube. From Figure 3.12, therefore we predict that DMF, acetonitrile and DMSO will not be able to form a nanotube. On the other hand, non-polar solvents like carbon tetrachloride would also have solvation problems and hence TAT-Im is more likely to precipitate out in this system.

3.3.2 DFT calculations for dimer and polymeric states

The dimer system consisted of two TAT-Im molecules and eight solvent molecules, as obtained from the crystal structure of TAT-Im in DCM. The dimer energy (E_2) for TAT-Im was then calculated as:

$E_2 = 0.5*$(Energy of dimer system-8*Energy of solvent)

Furthermore, we calculated the dimer stabilization energy (E_{12}) as the difference between E_2 and E_1.

Similarly, energy for the polymer system was calculated using periodic boundary conditions, and the corresponding stabilization energy was designated to be:

$E_{13} = E_3 - E_1$.

We hypothesized that the systems where both the dimer stabilization energy and polymer stabilization energy are negative would indicate the possibility of nanotube formation.

Solvent	E_{12} (kcal/mol)	E_{13} (kcal/mol)
Carbon tetrachloride	-41.46	-21.48
Chloroform	-31.48	-12.08
Ethyl acetate	-11.64	6.56
DCM	-21.46	-2.65
THF	-8.80	9.12
DMF	-143.72	-117.87
Acetonitrile	-4.94	12.94
DMSO	1.16	18.71

Table 3.8: DFT calculated dimer and polymer stabilization energies of TAT-Im in different solvent systems

The obtained values indicate the possibility of nanotube formation in carbon tetrachloride, chloroform, DCM and DMF. However, if we cross-reference this list with the results obtained in 3.3.1, the only remaining possibilities are DCM and chloroform. Interestingly, both these solvents not only contain weak hydrogen bond acceptors in the form of chlorine but also weak donors in the form of C-H group. This implies that the nanotube formation requires optimal interaction between solute and solvent – less interaction points to possible precipitation. In comparison, higher interaction may lead to solvent blocking the nanotube growth sites as seen in the experimental crystal structure of TAT-Im in DMF. Hence, we observe that the computational results are in agreement with the experimental crystal structures obtained so far, and conclude that optimal solute-solvent interaction is necessary for the formation of one-dimensional hydrogen-bonded nanotubes.

Chapter 4

Conclusion and Future Directions

To summarize, in Chapter 1 we discussed the types of organic nanotubes like carbon nanotubes, supramolecular nanotubes and covalent organic nanotubes. We looked at the pros and cons of carbon nanotubes and presented the need for developing a synthetic design for other forms of nanotubes. We then delved into the examples of supramolecular nanotubes in literature, and the use of large building blocks in most cases. Thereafter the importance of hydrogen bonding, especially weak hydrogen bonds, in supramolecular architecture was discussed.

In Chapter 2, the experimental procedures involved in the synthesis of the building block TAT-Im is shown. All schemes in the preparation of intermediates dinitrotriptycene, diacetamidodinitrotriptycene, diaminodinitrotriptycene and tetraaminotriptycene are presented. We also discuss the details of instrumentation for NMR spectroscopy, single-crystal X-ray diffraction experiments and IR spectroscopy. Furthermore, the setup of the computational DFT calculations and the choice of models are explained in detail.

In Chapter 3, the characterization of the intermediates is shown through their NMR spectra. The IR spectrum is also shown for TAT, along with its crystal structure. Finally, we present the crystal structures of TAT-Im in two different solvents, DCM and DMF, which show polymorphism. We then deliberate at length on the causes of the polymorphism based on the possible hydrogen bonding motifs from the crystal structure. Finally, we analyze the results of the DFT calculations and hypothesize that optimal interaction strength between the monomer and solvent is necessary for the formation of a one-dimensional nanotube, which is conveniently provided by weak hydrogen bonding.

This work therefore explores the possible type of interactions that case stabilize one-dimensional supramolecular structures like a nanotube. It especially highlights the conditions whereby a strong solute-solvent interaction results in premature termination of the hydrogen-bonded nanotube, resulting in short dimer or oligomer units. The experimental results will be extremely useful for designing other nanotubes in the future, and the computational results can be used as a stepping stone for crystal structure prediction (CSP) studies in the future[35].

I propose a design of a similar hydrogen-bonded nanotube from triptycene. The reaction of TAT with urea should form bis-cyclic urea with the triptycene core. This compound would have a unique blend of having hydrogen bond donors and acceptors perpendicular to each other, which can possibly result in the formation of a helical nanotube under suitable conditions.
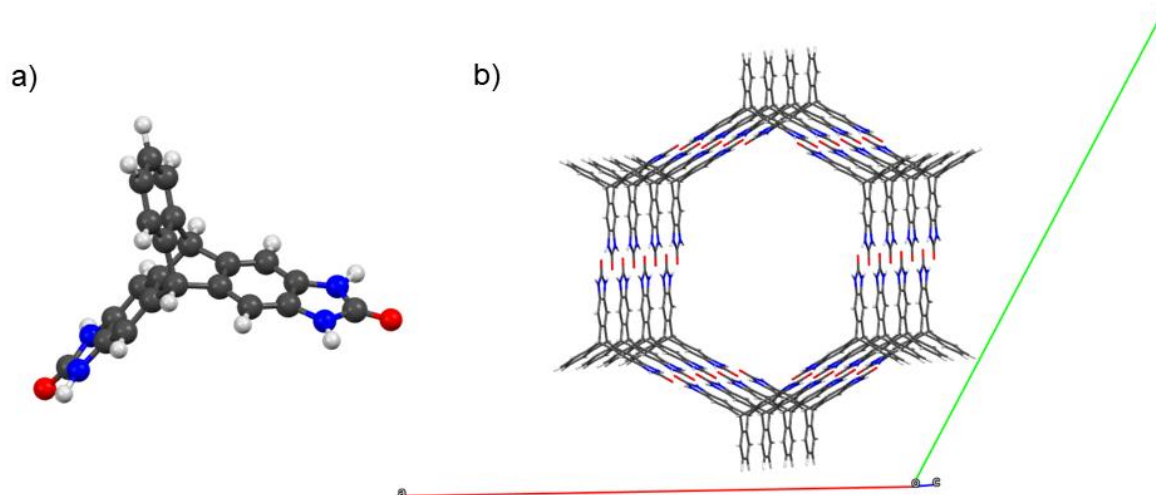
Fig.4.1: a) Cyclic bis-urea compound with triptycene core

b) Possible packing of the compound into a hexagonal nanotube

The synthesis and crystallization of this compound in different solvents alongside computational calculations, and comparison of results with this thesis, would further the understanding of the stability of hydrogen-bonded nanotubes.

References

(1) Iijima, S. Helical microtubules of graphitic carbon. *Nature* **1991**, *354* (6348), 56-58. DOI: 10.1038/354056a0.

(2) Oberlin, A.; Endo, M.; Koyama, T. Filamentous growth of carbon through benzene decomposition. *Journal of Crystal Growth* **1976**, *32* (3), 335-349. DOI: https://doi.org/10.1016/0022-0248(76)90115-9.

(3) Guo, T.; Nikolaev, P.; Thess, A.; Colbert, D. T.; Smalley, R. E. Catalytic growth of single-walled manotubes by laser vaporization. *Chemical Physics Letters* **1995**, *243* (1), 49-54. DOI: https://doi.org/10.1016/0009-2614(95)00825-O.

(4) Xiao-Di, W.; Vinodgopal, K.; Gui-Ping, D. Synthesis of Carbon Nanotubes by Catalytic Chemical Vapor Deposition. In *Perspective of Carbon Nanotubes*, Hosam El-Din, S., Said Moawad Mohamed, E.-S. Eds.; IntechOpen, 2019; p Ch. 2.

(5) Geckeler, K. E.; Premkumar, T. Carbon nanotubes: are they dispersed or dissolved in liquids? *Nanoscale Research Letters* **2011**, *6* (1), 136. DOI: 10.1186/1556-276X-6-136.

(6) Sweeney, S.; Hu, S.; Ruenraroengsak, P.; Chen, S.; Gow, A.; Schwander, S.; Zhang, J.; Chung, K. F.; Ryan, M. P.; Porter, A. E.; et al. Carboxylation of multiwalled carbon nanotubes reduces their toxicity in primary human alveolar macrophages. *Environmental Science: Nano* **2016**, *3* (6), 1340-1350, 10.1039/C6EN00055J. DOI: 10.1039/C6EN00055J.

(7) Yu, M.-F.; Lourie, O.; Dyer, M. J.; Moloni, K.; Kelly, T. F.; Ruoff, R. S. Strength and Breaking Mechanism of Multiwalled Carbon Nanotubes Under Tensile Load. *Science* **2000**, *287* (5453), 637-640. DOI: 10.1126/science.287.5453.637 (acccessed 2024/02/26).

(8) Zhou, M.; Wang, Z.; Wang, X. Chapter 5 - Carbon Nanotubes for Sensing Applications. In *Industrial Applications of Carbon Nanotubes*, Peng, H., Li, Q., Chen, T. Eds.; Elsevier, 2017; pp 129-150.

(9) Ma, L.; Dong, X.; Chen, M.; Zhu, L.; Wang, C.; Yang, F.; Dong, Y. Fabrication and Water Treatment Application of Carbon Nanotubes (CNTs)-Based Composite Membranes: A Review. In *Membranes*, 2017; Vol. 7.

(10) Peng, L.-M.; Zhang, Z.; Wang, S. Carbon nanotube electronics: recent advances. *Materials Today* **2014**, *17* (9), 433-442. DOI: https://doi.org/10.1016/j.mattod.2014.07.008.

(11) Ghadiri, M. R.; Granja, J. R.; Milligan, R. A.; McRee, D. E.; Khazanovich, N. Self-assembling organic nanotubes based on a cyclic peptide architecture. *Nature* **1993**, *366* (6453), 324-327. DOI: 10.1038/366324a0.

(12) Yu, Y.; Zhang, L.; Eisenberg, A. Morphogenic Effect of Solvent on Crew-Cut Aggregates of Apmphiphilic Diblock Copolymers. *Macromolecules* **1998**, *31* (4), 1144-1154. DOI: 10.1021/ma971254g.

(13) Fenniri, H.; Deng, B.-L.; Ribbe, A. E.; Hallenga, K.; Jacob, J.; Thiyagarajan, P. Entropically driven self-assembly of multichannel rosette nanotubes. *Proceedings of the National Academy of Sciences* **2002**, *99* (suppl_2), 6487-6492. DOI: 10.1073/pnas.032527099 (acccessed 2024/02/26).

(14) Shimizu, L. S.; Hughes, A. D.; Smith, M. D.; Davis, M. J.; Zhang, B. P.; zur Loye, H.-C.; Shimizu, K. D. Self-Assembled Nanotubes that Reversibly Bind Acetic Acid Guests. *Journal of the American Chemical Society* **2003**, *125* (49), 14972-14973. DOI: 10.1021/ja036515i.

(15) Pantoş, G. D.; Pengo, P.; Sanders, J. K. M. Hydrogen-Bonded Helical Organic Nanotubes. *Angewandte Chemie International Edition* **2007**, *46* (1-2), 194-197. DOI: https://doi.org/10.1002/anie.200603348.

(16) Pimentel, G. C.; McClellan, A. L. *The Hydrogen Bond*; W.H. Freeman, 1960.

(17) Desiraju, G.; Steiner, T. *The Weak Hydrogen Bond: In Structural Chemistry and Biology*; Oxford University Press, 2001. DOI: 10.1093/acprof:oso/9780198509707.001.0001.

(18) Varfolomeev, M. A.; Klimovitskii, A. E.; Abaidullina, D. I.; Madzhidov, T. I.; Solomonov, B. N. "Additive" cooperativity of hydrogen bonds in complexes of catechol with proton acceptors in the gas phase: FTIR spectroscopy and quantum chemical calculations. *Spectrochimica Acta Part A: Molecular and Biomolecular Spectroscopy* **2012**, *91*, 75-82. DOI: https://doi.org/10.1016/j.saa.2012.01.061.

(19) Desiraju, G. R. Supramolecular synthons in crystal engineering—a new organic synthesis. *Angewandte Chemie International Edition in English* **1995**, *34* (21), 2311-2327.

(20) Fabiola, G. F.; Krishnaswamy, S.; Nagarajan, V.; Pattabhi, V. C—H⋯ O Hydrogen Bonds in β-sheets. *Acta Crystallographica Section D: Biological Crystallography* **1997**, *53* (3), 316-320.

(21) Parra, R. D. Hydrogen-Bond-Driven Peptide Nanotube Formation: A DFT Study. In *Molecules*, 2023; Vol. 28.

(22) Scuderi, D.; Le Barbu-Debus, K.; Zehnacker, A. The role of weak hydrogen bonds in chiral recognition. *Physical Chemistry Chemical Physics* **2011**, *13* (40), 17916-17929, 10.1039/C1CP20987F. DOI: 10.1039/C1CP20987F.

(23) Hanessian, S.; Gomtsyan, A.; Simard, M.; Roelens, S. Molecular Recognition and Self-Assembly by Weak Hydrogen Bonding: Unprecedented Supramolecular Helicate Structures from Diamine/Diol Motifs. *Journal of the American Chemical Society* **1994**, *116* (10), 4495-4496. DOI: 10.1021/ja00089a056.

(24) Koner, K.; Karak, S.; Kandambeth, S.; Karak, S.; Thomas, N.; Leanza, L.; Perego, C.; Pesce, L.; Capelli, R.; Moun, M.; et al. Porous covalent organic nanotubes and their assembly in loops and toroids. *Nature Chemistry* **2022**, *14* (5), 507-514. DOI: 10.1038/s41557-022-00908-1.

(25) Dolomanov, O. V.; Bourhis, L. J.; Gildea, R. J.; Howard, J. A. K.; Puschmann, H. OLEX2: a complete structure solution, refinement and analysis program. *Journal of Applied Crystallography* **2009**, *42* (2), 339-341. DOI: doi:10.1107/S0021889808042726.

(26) Macrae, C. F.; Sovago, I.; Cottrell, S. J.; Galek, P. T. A.; McCabe, P.; Pidcock, E.; Platings, M.; Shields, G. P.; Stevens, J. S.; Towler, M.; et al. Mercury 4.0: from visualization to analysis, design and prediction. *Journal of Applied Crystallography* **2020**, *53* (1), 226-235. DOI: doi:10.1107/S1600576719014092.

(27) White, N. G.; MacLachlan, M. J. Soluble Tetraaminotriptycene Precursors. *The Journal of Organic Chemistry* **2015**, *80* (16), 8390-8397. DOI: 10.1021/acs.joc.5b01221.

(28) Kohn, W.; Sham, L. J. Self-Consistent Equations Including Exchange and Correlation Effects. *Physical Review* **1965**, *140* (4A), A1133-A1138. DOI: 10.1103/PhysRev.140.A1133.

(29) Becke, A. D. Density-functional exchange-energy approximation with correct asymptotic behavior. *Physical Review A* **1988**, *38* (6), 3098-3100. DOI: 10.1103/PhysRevA.38.3098.

(30) Lee, C.; Yang, W.; Parr, R. G. Development of the Colle-Salvetti correlation-energy formula into a functional of the electron density. *Physical Review B* **1988**, *37* (2), 785-789. DOI: 10.1103/PhysRevB.37.785.

(31) Becke, A. D. Density-functional thermochemistry. III. The role of exact exchange. *The Journal of Chemical Physics* **1993**, *98* (7), 5648-5652. DOI: 10.1063/1.464913 (acccessed 2/26/2024).

(32) Tomasi, J.; Mennucci, B.; Cammi, R. Quantum Mechanical Continuum Solvation Models. *Chemical Reviews* **2005**, *105* (8), 2999-3094. DOI: 10.1021/cr9904009.

(33) Mennucci, B.; Cancès, E.; Tomasi, J. Evaluation of Solvent Effects in Isotropic and Anisotropic Dielectrics and in Ionic Solutions with a Unified Integral Equation Method: Theoretical Bases, Computational Implementation, and Numerical Applications. *The Journal of Physical Chemistry B* **1997**, *101* (49), 10506-10517. DOI: 10.1021/jp971959k.

(34) *Gaussian 09 (Gaussian, Inc., Wallingford CT)*; 2009. (accessed.

(35) Woodley, S. M.; Catlow, R. Crystal structure prediction from first principles. *Nature Materials* **2008**, *7* (12), 937-946. DOI: 10.1038/nmat2321.